Computational Study of Ruthenium-Catalyzed Dimethylcarbamate Hydrogenation to Methanol: C-O and C-N Breaking Pathways [†]

Nils Estuardo M. E. Strand*

Department of Chemistry, University of Michigan, 930 North University Ave, Ann Arbor, MI 48109-1055

E-mail: strandn@umich.edu

Phone: +1 240.401.5297

[†]This thesis has been read and approved by Paul Zimmerman. Faculty advisor email: paulzim@umich.edu

ABSTRACT

CO_2-capturing methods have the potential to alleviate the adverse effects growing CO_2 amounts have on the Earth's atmosphere. The hydrogenation of CO_2 to methanol catalyzed by the Ru-MACHO-BH_4 complex, which includes a *PNP*-tridentate ligand, was studied using density functional theory (DFT) coupled with an automated reaction path finding tool. Initial coordination of dimethylamine to the electrophilic C(sp)-center of CO_2 led to the facile formation of the dimethylammonium dimethylcarbamate (DMC) salt, a key hydrogenation intermediate under basic conditions. After DMC formation a hydride transfer from the Ru center to the C(sp^2)-center in DMC resulted in the formation of dimethylformamide (DMF) and the release of water. Once DMF formed the carbonyl ligand bound to Ru was observed to accept an oxide ion from DMC thus playing a pivotal role in the cleavage of the C-O bond leading to dehydration of CO_2. Further analysis exposed an alternative pathway involving the formation of Ru-OH in response to the conversion of DMC to DMF prior to the liberation of water, leaving the carbonyl ligand out of the reaction. In either case, formation of MeOH would require the loss of the C-N bond in DMF which is energetically possible. However, careful study furthermore revealed the prospect of a C-O bond breaking pathway, which would not yield MeOH, but rather a mixture of trimethylamine (TMA) and water. C-O lability adds to the difficulty of selectively forming MeOH from CO_2 and so the careful investigation of the above pathways should lead to improvements in selectivity and conversion of CO_2 into MeOH.

CONTENTS

FIGURE LEGEND

1. INTRODUCTION

1.1. Motivation Behind CO_2 Reduction

Over several recent decades, the amount of carbon dioxide on the Earth's atmosphere has skyrocketed and is projected to continue increasing to levels which will bear detrimental consequences on the global climate.[1] One way to resolve this ongoing issue is to remediate emissions of carbon dioxide, namely through CO_2-capturing methods. This approach is of strong interest to many researchers, as it not only depletes the undesired species, but also allows for the formation of fuels such as alcohols.[2–4] Efforts have been made to convert CO_2 to more useful species using several approaches: (i) photoelectron-induced artificial photosynthesis; (ii) bulk electrolysis of a saturated solution of CO_2 via photovoltaics; (iii) hydrogenation of CO_2 using solar-produced H_2; and (iv) the thermochemical reaction of metal oxides and CO_2 at extremely high temperatures.

A number of investigations have been conducted to photochemically and electrochemically reduce CO_2 to CO, formate, or even methanol, using transition metal electrodes, metal complexes, semiconductors, and even organic materials as catalysts.[5–9] Photocatalysis, which makes use of a catalyst, photosensitizer, and sacrificial reductant, has traditionally been chosen as a convenient approach to reduce CO_2. Two primary challenges associated with this method, however, are that (i) there is little flexibility in acceptable redox potentials and (ii) it requires a catalyst/sensitizer pair with high stability in a number of oxidation states. The multicomponent photochemical reduction of CO_2 was explored to try to remediate these issues. Recent developments have shown that multinuclear systems can be employed to covalently link the sensitizer and catalyst via a bridgind ligand, leading to an inner-sphere electron transfer type interaction.[8,9] This new approach was found to yield vast improvements in various respects, including efficiency, durability, and kinetics.[10] Still, several limitations persist: (i) turnover numbers and turnover frequencies are far too low with frequently used

reductants such as triethanolamine or triethylamine; (ii) specific product selectivity, say of CO, formate, H_2, etc., is difficult to achieve; (iii) precious metal catalysts are often a necessity; (iv) organic solvents and sacrificial reagents are often required to overcome energy barriers associated with electron transfer; (v) reactions in aqueous solution require exact pH settings; and (vi) the required coupling between reduction and oxidation half-reactions can be difficult to achieve.

One strategy employed by Sato et al. involves the so-called Z-scheme, a process that describes the redox changes during light reactions of photosynthesis. The novel system revealed up to 70% selectivity for formate in the photoelectrochemical reduction of CO_2.[11–13] The system consists of a p-type InP semiconductor covalently bound to molecular ruthenium catalysts acting as the photocathode with TiO_2 as the photoanode. This advancement proved to be a major improvement over traditional systems, as it eliminated the need for a sacrificial reagent in aqueous solution. Ishitani and co-workers reported a successful artificial Z-scheme using Ag coupled with N-doped Ta_2O_5 (TaON) along with a Ru dinuclear complex (Ru_{photo} is directly attached to both the semiconductor and Ru_{cat}, which acts as the catalyst) to isolate the two-electron oxidation of methanol to formaldehyde from the CO_2 two-electron reduction half-reaction (**Figure 1**).[14] Complications arose from this study, however, as the reduction potential of Ru_{cat} proved high enough to aid in the electron transfer from the reduced Ru_{photo}, but it did not favor quenching of the excited state.

Despite these advancements hydrogenation remains a sought after method for CO_2 reduction. After all, hydrogen is considered a clean fuel with its high gravimetric energy density and its essentially nonexistent role in the global carbon cycle. In general, CO_2 hydrogenation has the potential to afford products classified as fuels, among which methanol represents an extremely important "hydrogen carrier"[15] that can be stored in bulk for further conversion to other organic material such as formaldehyde, olefins, dimethyl ether,[16] methyl *tert*-butyl ether, and acetic acid. Moreover, methanol can serve as a transportable liquid fuel and additive for fuel cells in the production of hydrocarbons, including synthetic gasoline. Refer

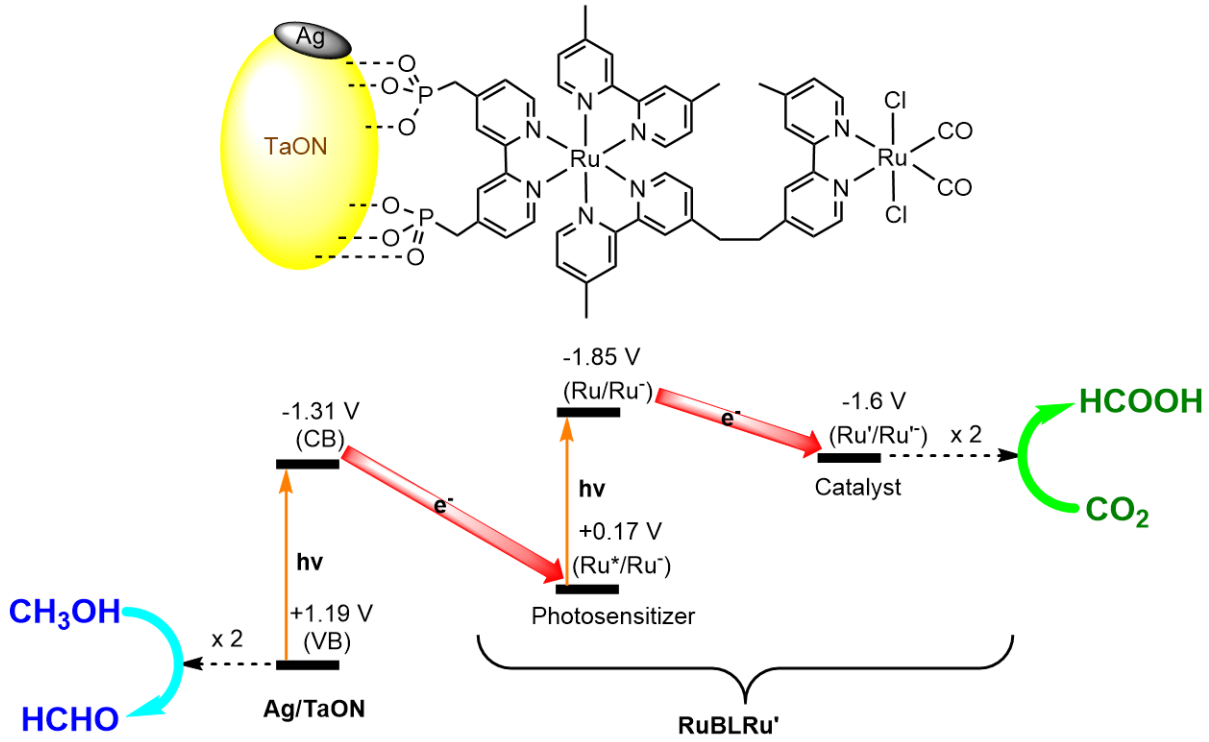

Figure 1: Photocatalytic CO_2 reduction Z-Scheme with methanol oxidation as the electron source. Adapted from reference 14.

to **Figure 2** for a list of useful products that can result from CO_2 hydrogenation, one such product being methanol.

1.2. Early Efforts in Hydrogenation Using Heterogeneous Catalysts

A large volume of work in CO_2 hydrogenation has revolved around the development of heterogeneous semiconductor catalysts to convert CO_2 to CH_3OH.[18–22] The attractiveness of heterogeneous catalysis stems from the relatively low cost of materials used and their high thermal stability. In addition, heterogeneous catalysts are of interest to researchers because they can easily be isolated from the products in the aftermath of a reaction, thus minimizing the loss of desired products resulting from separation methods. For example, Waller revealed the ability of a CuZnO semiconductor to catalyze the hydrogenation of CO_2 to form CO at 200 °C as well as CH_3OH at 180 °C. Each of the reactions were carried out at a reasonable

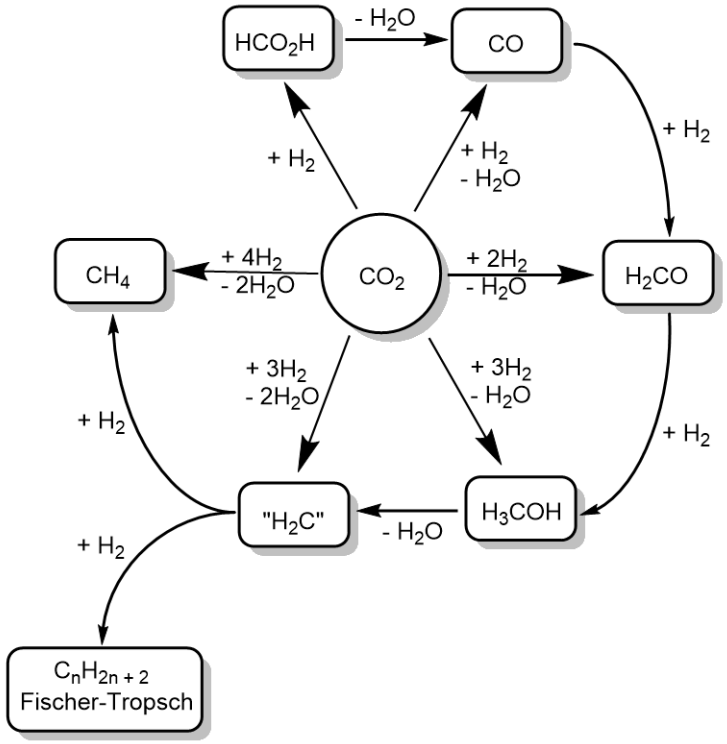

Figure 2: Hydrogenation of CO_2 as a source for industrially important products. Adapted from reference 17.

pressure (1 bar) for up to 205 minutes, yet the methanol yield proved to be quite low (0.2%).

One way to improve reaction kinetics, hence product yields, for these heterogeneous systems would then be to increase the reaction temperature above 200 °C, which is unfeasible given the highly positive entropy change associated with CO_2 hydrogenation. Furthermore, the heterogeneous approach tends to show low selectivity and unsatisfactory activity, resulting in extensive energy consumption.[23] It is also typical for heterogeneous catalysts to degrade over short periods of time as a result of low stability. It is necessary for the catalyst to be stable and to tolerate high temperatures in aqueous solution and it is for this reason that more efficient homogeneous catalysts are highly desired for CO_2 hydrogenation. The advantages of these species lie in their high activity, selectivity and flexibility, which then allows them to perform well in more benign conditions. Still, current research involving homogeneous catalysis is quite limited. Even though many efforts have successfully converted CO_2 to formic acid or to methanol via hydrogenation using homogeneous catalysis, only

very recently has this alternative approach been exploited to achieve reasonably efficient and selective CO_2 hydrogenation.[24–29]

1.3. Newest CO_2 Reduction Methodologies

1.3.1. Experimental

Many of the recent developments in CO_2 hydrogenation by homogeneous catalysis have involved catalysts with phosphine ligands. Over the last few decades, hydrogenation catalysts have been tweaked to allow incorporation of a wide variety of transition metals, including Ni, Pd, etc. with diphos ($Ph_2PCH_2CH_2PPh_2$) or other related phosphine-containing ligands. In 1993, Leitner et al. successfully carried out the reduction of CO_2 to formic acid in aqueous solution using a rhodium-phosphine complex at room temperature.[24] The highest turnover number of 3440 was achieved with $RhCl(tppts)_3$ (tppts = tris(3-sulfonatophenyl)phosphine). In another study by Joó et al., turnover frequencies for CO_2 hydrogenation to formic acid reached values as high as 9600 h^{-1} at 80 °C and 9.5 Mpa H_2/CO_2 using $[RuCl_2(tppms)_2]_2$.[25] Laurenczy et al. discovered that iridium and ruthenium complexes containing the water-soluble PTA ligand were capable of catalyzing this reaction as well.[26–29] Through these studies it was found that hydrogen bonding interactions between the phosphine ligands and the bicarbonate substrate facilitated hydride transfer.

One of the ultimate goals in improving conditions for CO_2 hydrogenation is to eliminate the exclusive reliance on precious metals. Reports of successful usage of nonprecious metal catalysts are scarce. One of the first to carry out this transition, Beller and co-workers were some of the first to report nonprecious metal catalyzed hydrogenation of CO_2 to bicarbonate using $Co(BF_4)_2)\cdot 6H_2O$ with the PPh_3 ligand in 2012 ($PPh_3 = P(CH_2CH_2PPh_2)_3$). Experimental data releaved a high TON of 3877 and a remarkably improved catalytic ability compared to other nonprecious-metal systems.[30] They later reported the same reaction using a thermally stable and active iron(II) complex, iron(II) fluoro-tris[(2-(diphenylphosphino)phenyl)phosphino]-

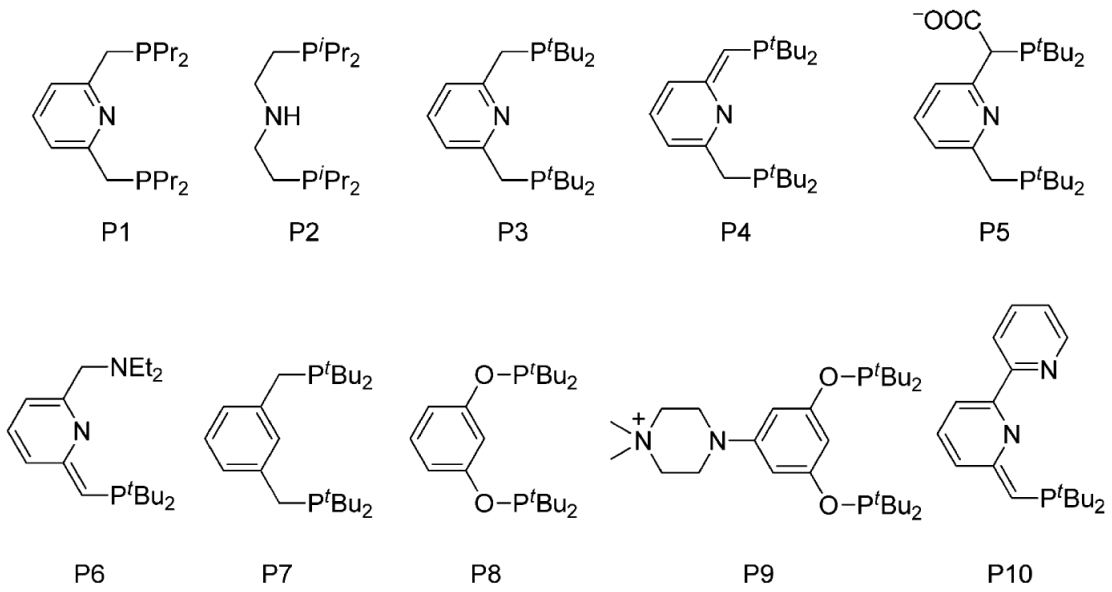

Figure 3: Pincer ligands used for complexes involved in CO_2 hydrogenation to formate, as well as formic acid dehydrogenation.

tetrafluoroborate, at 100 °C under 6 MPa H_2, this time with a TON over 7500.[31]

Some of the more recent work in the field has involved metal complexes with pincer ligands (**Figure 3**). In 2011, Hazari and co-workers reported CO_2 hydrogenation using an air-stable, water-soluble Ir-based catalyst, IrH_3(P2) (P2 = (diisopropylphosphinoethyl)amine) (**Figure 3**). The specific pincer ligand used in this study contained an N-H group, which was found to interact with the formate substrate via hydrogen-bonding. It is clear from this work that this ligand feature proves pivotal toward good catalyst performance as the resulting intermediate, Ir(OCHO)-H_2(P2), facilitated the hydride transfer step, thus contributing to a much improved TON of 348000.[32] A Ru pincer complex with a similar N-H group, [Ru(P2)(H)(Cl)(CO)] (**Figure 4**), was used by Ding et al to catalyze the hydrogenation of ethylene carbonate and other cyclic carbonates as well as polycarbonates to methanol at a reasonable 50 atm H_2 and 140 °C.[33] The group theorized that the N-H group contributes to to proton transfer through hydrogen bonding with the carbonyl substrate.

There is no doubt that conversions of CO_2 and H_2 to MeOH and other related fuels are thermodynamically favorable reactions. Still, many of the catalysts to date remain limited

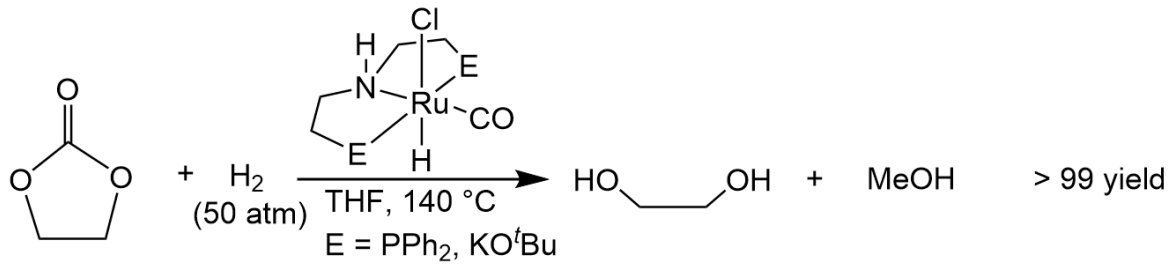

Figure 4: Methanol production from Ru-pincer-catalyzed ethylene carbonate hydrogenation. Adapted from reference 33.

by the requirement for impractical and expensive hydrogen sources such as boranes and hydrosilanes.[34] Indeed, not many reports using single molecular catalysts exist in the literature. Given that the synthesis of MeOH from CO_2 in one step is considered to be a difficult task, Sanford and co-workers engineered a Ru-based system to catalyze the conversion of CO_2 and H_2 to formic acid, methyl formate, and eventually MeOH. This cascade catalysis system consists of three Ru complexes operating in tandem as well as one separate catalyst coupled with $NHTf_2$.[34] The main advantage of this system is that the rate and selectivity of each step of the overall reaction can be fine-tuned by varying the catalyst from step to step. However, this can come with a price, namely that the catalysts are not necessarily compatible with one another. The main side reaction identified was esterification and the best turnover number achieved at 135 °C for the formation of MeOH was merely 2.5. Still, this value increased to 21 upon separating catalysts **A** and **B** from catalyst **C** by placing them in two separate vessels, so as to avoid contamination of **C** by $Sc(OTf)_3$ (**Figure 5**).

While a number of experimental studies has been devoted to designing molecular catalysts for the selective hydrogenation of CO_2, one should not disregard the theoretical studies performed in recent years to explore and uncover reaction mechanisms responsible for these transformations. In the next few paragraphs, we outline some of the most imporant theoretical contributions to the study of CO_2 hydrogenation.

1.3.2. Computational

Among the various computational studies on the reaction mechanisms published for CO_2

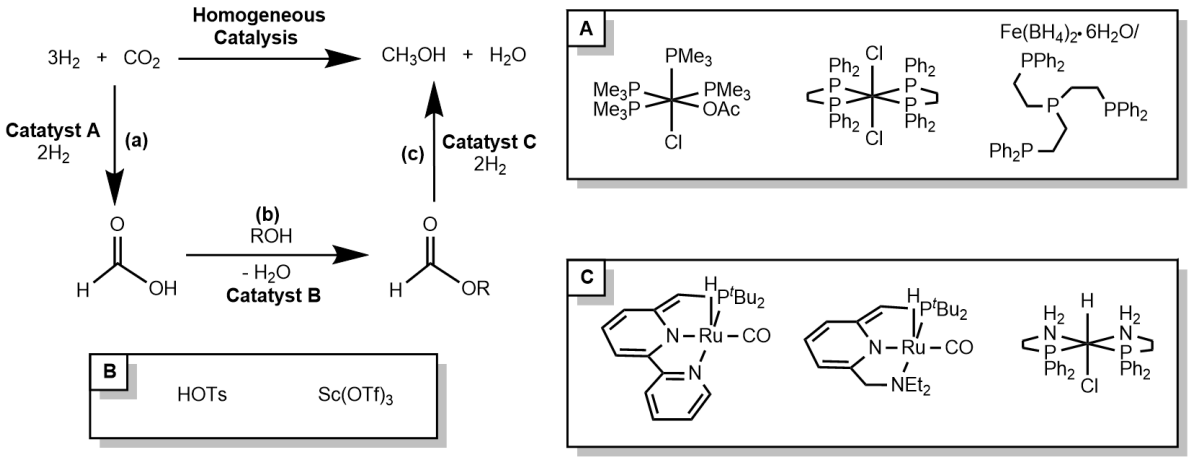

Figure 5: CO_2 hydrogenation to MeOH via cascade catalysis and catalysts used. Adapted from reference 34.

hydrogenation, a very recent mechanistic study using density functional theory (DFT) carried out by Appel and co-workers involved the complex $Co(dpme)_2H$. Results revealed a reaction pathway that begins with the binding of the carbon atom in CO_2 to the cobalt center, resulting in an octahedral $Co(dpme)_2(H)(CO_2)$ precursor, which in turn allows for facile hydride transfer from Co to the electrophilic CO_2 carbon.[35] The same study suggested that direct hydride transfer from cobalt to an approaching CO_2 substrate is also feasible given that the activation barrier of this pathway is only 1.4 kcal/mol higher in energy than the CO_2-cobalt adduct pathway.

Computational studies have also been performed by Pidko et al. on the very successful RuH(Cl)(CO)(P3) (P3 = 2,6-bis(di-*tert*-buthylphosphinomethyl)pyridine, **Figure 3**), which was shown experimentally to hydrogenate CO_2 to formate with a turnover frequency as high as 1100000 h^{-1}.[36,37] The works revealed that the catalyst transforms into a bis-hydrido Ru complex, $[Ru(H)_2(CO)(P3)]$, which is speculated to be the active species for hydrogenation, whereas the ligand-assisted CO_2 adduct is actually deemed to be inactive. It turned out that any reaction pathways involving interactions between metal center and substrate led to high activation barriers or unstable intermediates; meanwhile, catalytic cycles which do not include binding of the CO_2 substrate to the metal are active, with lower barriers to

hydrogenation (**Figure 6**).

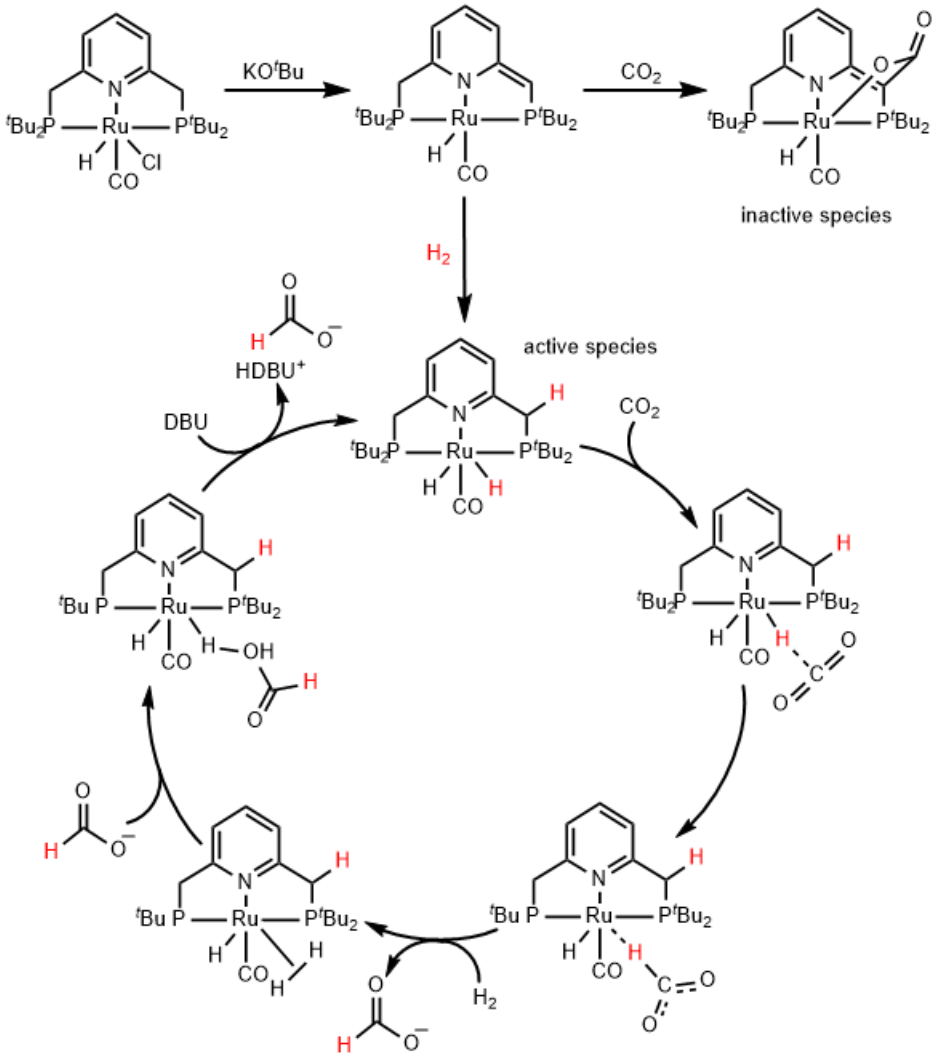

Figure 6: Suggested catalytic cycle for CO_2 hydrogenation to formate catalyzed by RuH(Cl)(CO)(P3). Adapted from reference 37.

In another set of DFT studies by Suna et al. and Hou et al. H_2 heterolysis catalyzed by two different Ir-based catalysts, [Cp*Ir(4DHBP-2H$^+$)] and [Cp*Ir(6DHBP-2H$^+$)] (nDHBP = n,n'-dihydroxy-2,2'-bipyridine), were studied. It was found that both systems lead to an iridium hydride intermediate whose formation was shown to be the rate-determining step.[38] It was found that the [Cp*Ir(6DHBP-2H$^+$)] complex contained a basic oxyanion which lowers the activation free energy of H_2 heterolysis, and agrees with the improved reaction rates

detected experimentally. The elucidated mechanism suggests that insertion of CO_2 into the Ir-H bond is possible. It was later suggested by Hou et al. that formic acid formation involves the process of "ligand assisted hydride transfer" at an even lower activation barrier for the 6DHBP complex.[39]

In a separate computational study involving a different iridium-based catalyst, Hazari and co-workers showed that substrate-ligand H-bonding interactions possible with the presence of an N-H group lowers the activation barrier of the reaction, and makes the product more thermodynamically favorable.[32] DFT calculations validated the hypothesis that the N-H group present in the iridium complex rendered CO_2 insertion much more energetically favorable, as the mechanism suggests the formation of a stable N-H-O hydrogen bond through an outer-sphere reaction. The calculations reveal that inserting CO_2 to the complex leads to a formate intermediate interacting with the ligand via hydrogen bonding.

In addition, some important computational work has been accomplished in the realm of CO_2 hydrogenation to formic acid catalyzed by nonprecious metals. The reaction mechanism using the iron complex $[FeH(PP_3)]^+$ ($PP_3 = P(CH_2CH_2PPh_2)_3$) as the catalyst was identified via DFT by Yang et al.[40] β-hydride elimination was identified as the rate-limiting step, the activation barrier being more favorable than that of a potential neutral pathway beginning with direct hydrogen transfer from HCO_2^- to the iron center. Later, the same group conducted one promising study elucidating the mechanism of dimethyl carbonate hydrogenation to MeOH catalyzed by a Ru-*PNP*.[41] Prior to this, other groups such as that of Milstein proposed mechanism for the hydrogenation of dimethyl carbonate, as shown in **Figure 7**.[42] Yang proposed three cascade catalytic cycles involving the splitting of three H_2 molecules and the subsequent formation of the three MeOH molecules throughout the overall conversion of a number of substrates, including dimethyl carbonate, but also methyl formate, and formaldehyde, to MeOH. Close analysis of energetics involved in this reaction allowed for the design of a new iron pincer complex as the catalyst, [*trans*-(PNN)Fe$(H)_2$(CO)], which was found to have an activation barrier that was 3.4 kcal/mol lower in energy than the

original catalyst.

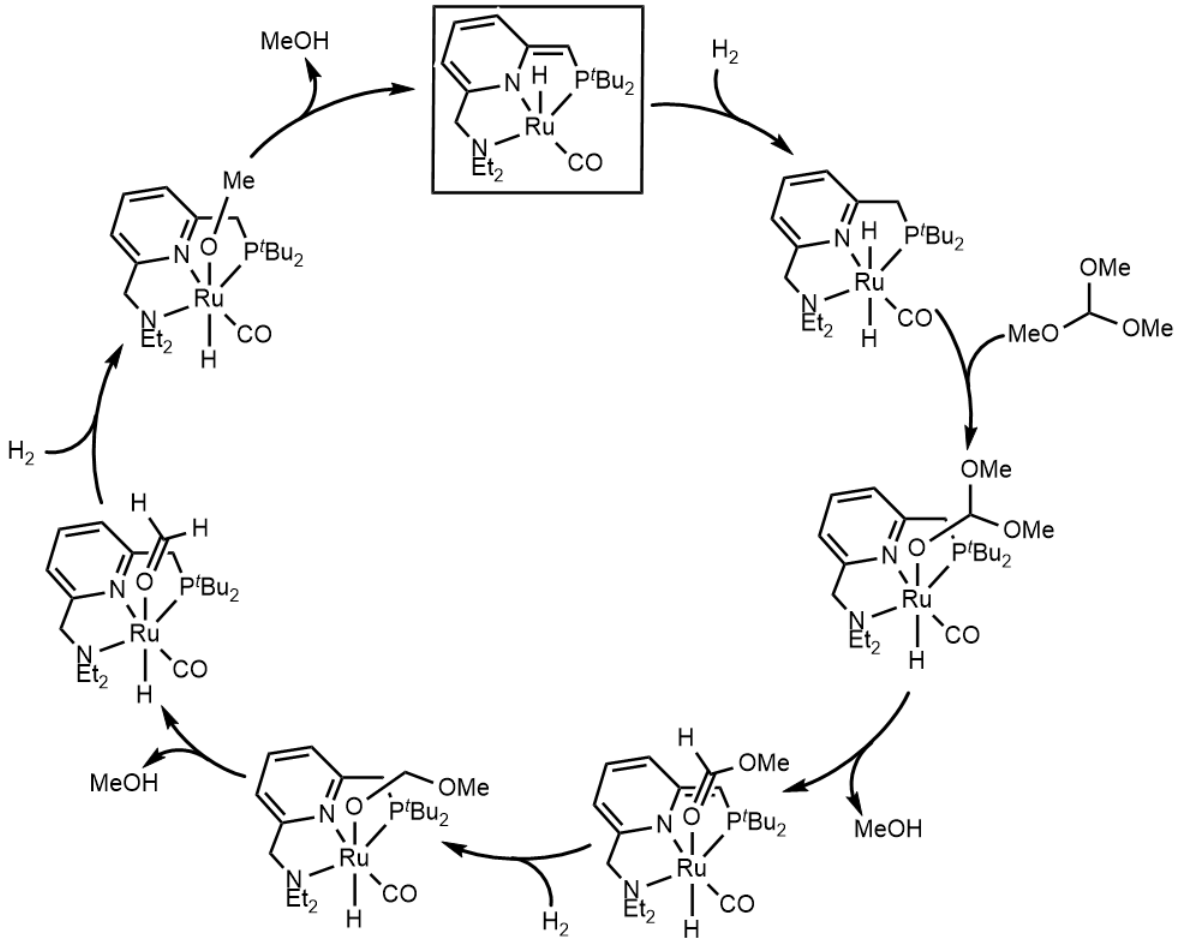

Figure 7: Proposed mechanism for Ru-catalyzed dimethyl carbonate hydrogenation to MeOH. Adapted from reference 42.

1.4. Limitations in Current Hydrogenation Studies

There is no doubt that the mechanism for the hydrogenation of dimethyl carbonate discussed in the previous subsection represents to date one of the most closely studied selective hydrogenation pathways of sp^2C-containing compounds to methanol using DFT. Still, the mechanism for the conversion of CO_2 to dimethyl carbonate is not well known. Similarly, the direct synthesis of dimethyl carbonate from CO_2 has also proved intractable, thus limiting

the potential application of this intermediate for the indirect production of MeOH from CO_2.

The systems identified in the previous subsection for the conversion of CO_2 to formic acid, and eventually to methanol, operate under acidic conditions, and are thus incompatible with the bases typically utilized for CO_2 capture.[2–4] While there exist numerous technologies compatible with the carbon capture and storage process, only a few have been labeled as acceptable for commercial deployment in industrial settings. The options that are considered feasible even to date are post-combustion CO_2 capture in the presence of basic solvents, particularly amines. In a typical amine-based CO_2 capture system, a steady stream of CO_2 is combined with an aqueous solution of amine, inciting a reversible reaction between CO_2 and the basic solvent to form salts which dissolve in water. It is for this reason that basic amines are so suitable for state of the art carbon capture technologies. The integration of current reactions involving selective CO_2 to MeOH reduction, which typically involve formic acid as an intermediate, with reasonable carbon sequestration methods of the modern era has proved to be a real challenge.

1.5. Basic CO2 Reduction: Organic Synthesis Background

The incompatibility between CO_2 capture and hydrogenation noted in the previous subsection led Sanford and co-workers to propose an alternative method for hydrogenating CO_2 to MeOH under basic conditions involving the initial combination of CO_2 with an amine to form a carbamate salt followed by Ru-*PNP*-catalyzed conversion of the carbamate to the desired species in a multi-step process, as shown in **Figure 8**.[43] This novel system involves the combination of dimethylamine ($NHMe_2$) and the ruthenium complex, which in tandem catalyze the hydrogenation of CO_2 to a mixture of dimethylformamide (DMF) and MeOH with up to 96% of the CO_2 being converted to products.

The system studied by Sanford uses dimethylcarbamate (DMC), which can be formed from the reaction of CO_2 with two equivalents of $NHMe_2$, as a starting point. However, a few requirements had to be taken into consideration. For one, DMC has a carbonyl group whose

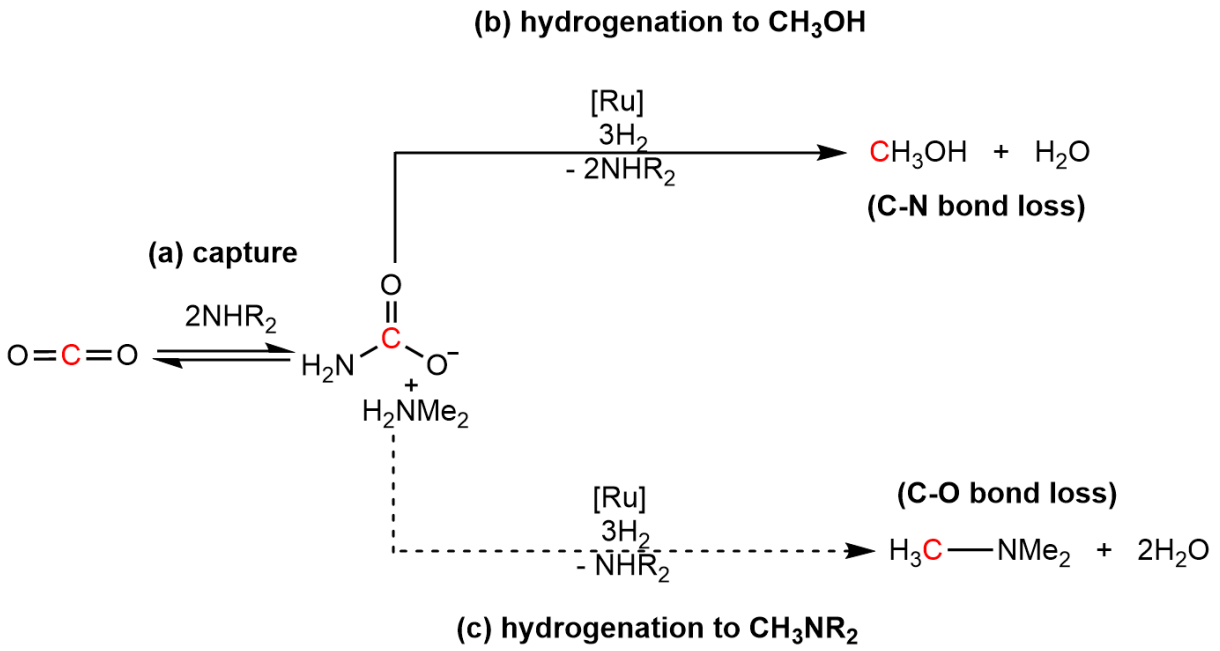

Figure 8: Proposed steps for CO_2 hydrogenation catalyzed in tandem by Ru complex and $NHMe_2$. Adapted from reference 43.

electrophilicity is particularly low, meaning the catalyst must be highly reactive toward the C(sp^2)-center. Moreover, the base used for this process, $NHMe_2$, will be present in solution, meaning the catalyst must be stable under basic conditions. Additionally, the catalyst must be selective toward C-N bond cleavage over C-O bond cleavage, as it is possible for trimethylamine (TMA) to form instead of MeOH. Three catalysts were able to work under these constraints, namely **3**, **5**, and **6** (**Figure 9**). DMC was reacted with 1 mol % of each catalyst at 155 °C in THF under 50 bar H_2 and was successfully converted to MeOH using all three catalysts. **6** (Ru-MACHO-BH_4) achieved a TON of 19, the highest of the three. Even this TON value, however, is far too low for this system to be deployed to a fully commercial setting. Moreover, the **6**-catalyzed reaction required the addition of 50 equivalents of K_3PO_4 in order to reach that TON value. Without this reagent, the TON using **6** was only 3.

Further refinement of the catalytic protocol devised by Sanford and co-workers necessitates a thorough understanding of the origins of chemical selectivity. We herein report the use of theoretical and computational methods to explore the factors leading to the limited

extent of methanol formation using catalyst **6**, as observed experimentally. In the following subsection, we first describe the theoretical foundations of quantum chemistry that lie at the heart of our methodology and subsequently outline the relevant details of the computational tools that we employ. Finally, we discuss the details of the catalytic cycle(s) elucidated using DFT.

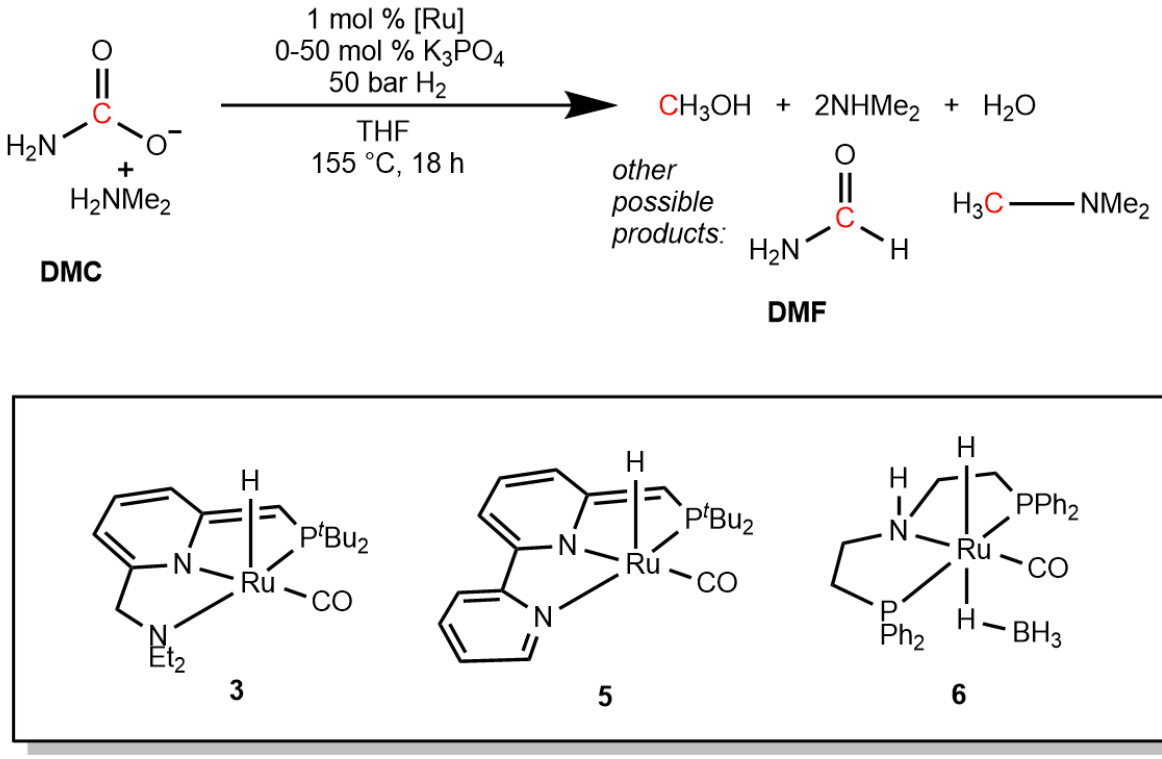

Figure 9: Reaction scheme representing the basic hydrogenation of DMC to MeOH. Adapted from reference 43.

1.6. Theoretical Chemistry Background

1.6.1. Motivation Behind Theoretical Methods

One of the biggest building blocks toward understanding chemical selectivity is the reactive landscape that results from the relationship between energy and position, whose dimensionality depends on the number of relevant degrees of freedom, which comprise quantities

such as bond lengths, angles, and torsions. This landscape contains a large volume of chemical species, including reactants, products, transition states, and intermediates. If one takes a simple chemical process such as water autoionization, one of the dimensions of the landscape would correspond to the O-H-O bond axis of two adjacent water molecules.

The more complex a system, the more degrees of freedom exist in the reactive space associated with the reaction of interest. Although the resulting landscape often becomes multidimensional, it is possible to visualize it as a "potential energy surface," essentially a two-dimensional cross-section of the landscape. In a typical one-step reaction, such as the formation of product **C** from reactants **A** and **B**, the combination of **A** and **B** are initially located in a valley somewhere along the surface. Likewise, in the aftermath of the reaction, **C** can be found at a different valley. This must mean that somewhere along the reaction path, there has to be a maximum energy point. This "saddle point" represents the transition state of the reaction. Understanding the potential energy surface allows us to uncover from first principles kinetic and thermodynamic details regarding the reaction of interest. Quantum mechanics allows for the construction of potential energy surfaces for use in studying chemical reactions.[44]

This is done using quantum mechanical wave functions (Ψ), from which it is possible to mathematically construct all of the pieces of information that make up the current state of a system. One of the most paramount relationships in quantum mechanics is the Schrödinger equation, a classic eigenvalue problem. It essentially equates the operation of the Hamiltonian ($\hat{H}$) on the wave function, the eigenfunction, to the product of the energy (E) and the same wave function:[44]

$$\hat{H}\Psi = E\Psi \tag{1}$$

Solving this equation allows us to construct the sough-after landscapes that describe chemical systems.

Unfortunately, exact solutions to the Schrödinger cannot be obtained analytically for systems beyond the simple hydrogen atom, rendering the construction of accurate reactive

landscapes a real challenge for the majority of chemical systems. Over time, however, methods of obtaining approximate solutions for the generation of complex reactive landscapes have been devised. One such technique, Density Functional Theory (DFT),[44] has emerged as a particularly convenient panacea to the intractability of quantum problems, as it represents an ideal balance between computational effort and accuracy of results for a large variety of systems.

1.6.2. Density Functional Theory and Reactive Landscapes

DFT was devised in 1964 by Walter Kohn and Pierre Hohenberg in efforts to efficiently and accurately compute the ground-state electronic energy of a molecular system. The novel technique makes use of a mathematical construct called density funcitonal, which describes the energy resulting from electron density in standard three-dimensional Cartesion coordinates. The success of DFT stems from its ability to approximately solve the Schrödinger equation without relying on mathematically intractable wave functions.[45]

The invention of DFT coupled with recent improvements in method development and available computational power has helped to establish a means for fast and reliable computation of chemical information. These methods have provided a robust platform for a large variety of electronic structure calculations involving highly complex systems. Advances in methods and computational power have aided in solving the problem of searching a reactive landscape for useful reaction pathways. Many quantum chemistry computational software packages such as Q-Chem[46] that exist today are designed to perform calculations to unearth reactive landscapes involving a wide variety of chemical transformations.

With a means to efficiently and effectively generate reactive landscapes from state of the art DFT methods, we now seek methods to navigate through landscapes to extract useful information regarding specific chemical reactions. Ideally such a method would yield a one-dimensional trajectory that begins at the valley consisting of reactants **A** and **B** and ends at the valley for intermediate **C** and passes through a transition state. Because the overall energy of the path must be minimized, the transition state must lie on a saddle point within

the potential energy surface. Historically, the process of locating transition states of reactions via DFT has proved computationally challenging and has necessitated a considerable amount of chemical intuition from a human perspective.[47] With the development of Growing String Method (GSM),[48,49] efforts to search for transition states along a landscape have become significantly more facile.

Initially, GSM was classified as a double-ended reaction path search algorithm (DEGSM). This version of the method required the input of both start and end input geometries to compute the exact transition state structure connecting the two endpoints of the pathway. A more recent variant of the method, single-ended growing string (SEGSM), requires the input of the starting structure along with driving coordinates, changes in chemical bonds and angles that define a reaction path of interest, and finds transition states and intermediates for elementary reaction steps without prior knowledge of the exact product structure. The general algorithm for SEGSM and its visualization along a contour map are displayed in **Figure 10**. The first step in the reaction path finding process is to optimize the geometry of the starting structure via DFT. Next, SEGSM takes the DFT-generated potential energy surface and searches for a reaction path by generating and optimizing nodes along the search direction defined by the driving coordinates. A transition state is eventually located as the string progresses over a high energy point and continues back downhill toward an intermediate or final product structure. Finally, all nodes along the reaction path are individually optimized to generate the final string containing the exact transition state.

Two powerful tools, DFT and GSM, can hence be combined together to reveal insightful information relevant to chemical systems, such as thermodynamics and kinetics of elementary steps. The following subsection outlines our purpose for using these methods in our current study and the goals we set regarding the elucidation of **6**-catalyzed CO_2 hydrogenation to methanol under the presence of $NHMe_2$.

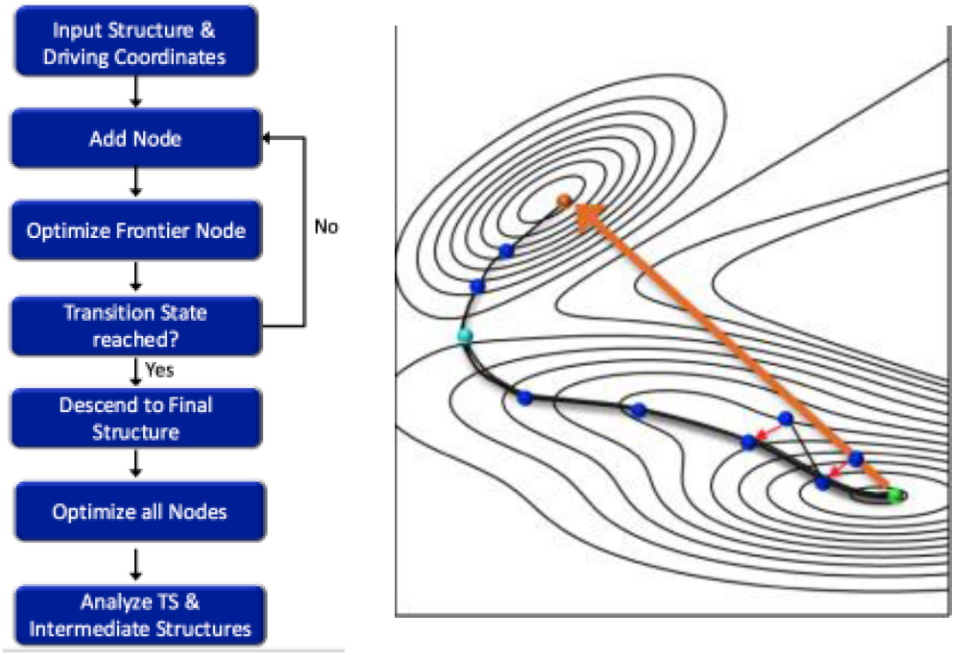

Figure 10: Schematic diagram of the SEGSM method (left); transition state search algorithm as shown on a contour plot (right). Each node along the reactive landscape is individually identified as shown by the arrows.

1.7. Goals for Studying Ru-catalyzed CO_2 Hydrogenation with DFT

To overcome the challenge of limited catalysis associated with the reaction converting CO_2 to MeOH in the presence of $NHMe_2$, it was crucial to computationally examine the possible reaction mechanisms for DMC conversion to MeOH using **6**. We made use of the single-ended Growing String Method (SEGSM),[47] which, as explained in the previous subsection, uses DFT to obtain reaction paths corresponding to input structures and driving coordinates for potential reaction paths. The elucidated reaction paths reveal both transition state structures as well as intermediate structures for energetically feasible pathways. A separate method, ZStruct, was used prior to each SEGSM execution to generate the possible driving coordinates, namely combinations of bond-adding and bond-breaking occurrences between reactive atoms as designated by the user, as well as changes in bond angles, in a systematic way.[50] ZStruct was also capable of aligning reactant species for input in reaction path searches. Because the reaction path search process only requires knowledge of the

starting structures and reactive atoms in each reactant, ZStruct and SEGSM can together search a wide span of reaction space in an automated fashion.

The power of ZStruct stems from its ability to systematically drive either intramolecular or intermolecular reactions given the input of basic chemical structures. For the combination of catalyst and substrate, for instance, the method generates a combinatorial set of driving coordinates and aligns the structures for each driving coordinate generated before feeding each combined structure/driving coordinate to GSM for subsequent transition state and intermediate finding.[51] Intermediates obtained from this process are themselves then used for the next ZStruct run and the process is repeated until a full reaction network has been constructed.[52] ZStruct has been shown to function well with systems containing more than 100 atoms, with as many as 15 labeled as active.[53] Careful separation of atoms that are reactive is crucial since running the method on large systems with a high number of reactive atoms would otherwise generate more driving coordinates than could be feasibly computed.

We now have a complete description of the methodology that was used extensively to examine the reaction mechanism for basic CO_2 hydrogenation. Goals of the study included obtaining a set of full catalytic cycles for the reaction of interest, while also identifying any side reactions which could potentially hinder the conversion of DMC to MeOH, such as the cleavage of the C-O bond in DMC resulting in NMe_3 formation. In order to speed up initial mechanistic studies, the number of atoms in the system was decreased by replacing Ph groups on the Ru complex with Me groups. This smaller model allowed for a base mechanistic understanding while still identifying the full pathway. During each step in our pathway, the roles of H_2, dimethylamine, and the dimethylammonium ion were each evaluated.

2. COMPUTATIONAL DETAILS

All quantum chemistry calculations were performed by DFT with the Q-Chem quantum chemistry package. For gas-phase calculations LANL2DZ was chosen as the basis set as well as the ECP on ruthenium along with B3LYP as the density functional. For all elementary steps considered, ZStruct was initially used to generate driving coordinates and substrate alignments prior to executing SEGSM, which was subsequently used to simultaneously find the minimum energy path and exact transition state by an unconstrained saddle point search at the highest energy node within the string. Entropic and enthalpic corrections were applied to the gas-phase energies at a temperature of 155 °C.

3. RESULTS AND DISCUSSION

3.1. Overall Methodology and Summary of Mechanisms

The initial CO_2 capture step involving the formation of dimethylammonium dimethylcarbamate (DMC) was studied via DFT. The reaction was determined to proceed in two parts: (i) the formation of a C-N bond resulting from the binding of $NHMe_2$ to CO_2, and (ii) the proton transfer from the Lewis adduct to a second $NHMe_2$ molecule. The formation of DMC from CO_2 and $NHMe_2$ proved quite facile, given that gas-phase activation barrier and Gibbs free energy change were computed to be 0.2 kcal/mol and -6.0 kcal/mol, respectively. The subsequent reactions involving DMC, H_2, and the ruthenium catalyst are, however, much more complex. Due to the anticipated intricacy and unknown nature of these reactions, our automated reaction finding tools were used to locate the key chemical transformations. These methods enable the discovery of reaction pathways from a given set of reactants by systematically applying changes to the connectivity between specified atoms in both reactants. Additional reagents such as H_2 and $NH_2Me_2^+$ are added to the simulation at relevant steps and the process is repeated until full pathways to product formation and catalyst regeneration are found. Of course, not all mechanisms will be perfectly valid, even if they include the formation of the desired product (e.g. methanol). For one, it is crucial that the catalyst revert back to its original form at the end of one cycle. Second, the activation barrier should not exceed an approximated threshold. This value can be computed with the help of the following equation:

$$\frac{\Delta G_1^{\ddagger}}{T_1} \propto \frac{\Delta G_2^{\ddagger}}{T_2} \tag{2}$$

where $\Delta G_1^{\ddagger}$ and $\Delta G_2^{\ddagger}$ represent expected activation energies at temperatures T_1 and T_2 in Kelvin, respectively. Assuming that the energy barrier of a kinetically unfavorable (low-rate) reaction at room temperature (298 K) is roughly 25 kcal/mol or higher, this threshold at 155 °C (428 K), which was the temperature chosen experimentally for this reaction,[43] is

calculated to be 39 kcal/mol. Hence if, after corrections for enthalpy/entropy contributions resulting from frequencies, the overall transition state energy for a particular catalytic cycle exceeded the starting energy by more than this amount, we assumed that this pathway is unlikely to occur.

While it can be said that ZStruct tremendously reduces the amount of human effort and chemical intuition necessary for the successful execution of GSM, some amount of human reasoning is required to avoid analyzing pathways that are redundant or extraneous from the reaction of interest. It is for this reason that for each elementary step, we made sure to identify specific atoms of our system which are reactive. In this way, ZStruct only generates driving coordinates for atoms that are labeled as reactive, thus significantly reducing the number of pathways sampled. Even with a truncated set of GSM executions, however, one can still reduce this number even further, by not only identifying reactive and unreactive atoms, but also distinguishing relevant bond-adding and breaking occurrances from non-relevant ones. For instance, if methanol is the product of interest, the loss of two C-O bonds in DMC would be unfeasible, yet cleavage of the C-N bond would be essential. It was crucial to note that a maximum of two add moves and break moves each are allowed for each execution of GSM. Throughout our reaction searches the dissociation of the carbonyl ligand from Ru was found to be high in energy (barriers up to 80 kcal/mol) and therefore these pathways were disregarded from further studies. The stability of this ligand when bound to the ruthenium center suggests that it likely plays an important role in interactions between the catalyst and the DMC substrate. It was also important to carefully single out the species to introduce to the reactive medium at each step. For instance, introducing H_2 can help drive the reaction forward particularly if the Ru complex is hydride-deficient, even though sometimes adding H_2 will fail to lead to any attractive intermediate. Similarly, addition of $NH_2Me_2^+$ would be beneficial if, for example, protonation of a hydroxy ligand would result in the loss of water, which is a necessary step as noted in **Figure 2**. From the scheme laid out in **Figure 2** one can also deduce that only three H_2 molecules are needed

throughout the catalytic cycle. We kept each of the above considerations in mind when carefully identifying relevant reagents and driving coordinates prior to each elementary step.

Multiple catalytic cycles were generated from the methodology described above, clearly showcasing the combined power of ZStruct and SEGSM. A summary of energetics associated with all cycles is shown in **Table 1**. The combination of the initial ruthenium complex (**1**) with DMC was explored via SEGSM. Even though more than one hundred transition states were identified, one pathway of interest was singled out, as it revealed the formation of dimethylformamide (DMF), one of the side products detected experimentally. The reaction step resembled a σ-bond metathesis mechanism, with one of the hydrides attached to Ru taking the place of one of the oxide ions in DMC. The oxide subsequently shifted from the metal center to the carbonyl ligand, stabilizing the resulting complex (**2**). This interaction helps corrobrate the potential importance of the carbonyl ligand in generating feasible pathways for MeOH formation.

We hypothesized DMF is a potential intermediate toward methanol formation. After all, this step involves the formation of a C-H bond, two more of which are needed to produce MeOH. Moreover, the loss of one C-O bond is promising because MeOH only contains one of the two C-O bonds initially present in the complex. Hence it was important to repeatedly execute SEGSM on the new species to assess whether MeOH formation was possible from this pathway, and if so, compare energetics involved with formation of DMF, whether an intermediate or final product, or some different final product such as MeOH or TMA.

3.2. Catalytic Cycle 1: MeOH and TMA Pathways

As anticipated, a full catalytic cycle was generated for the formation of MeOH with DMF as an intermediate (**Cycle 1**, **Figure 11**). Binding of the oxygen atom in DMF to the ruthenium center resulted in hydride transfer from Ru to the C(sp^2)-center to form **3**. Release of (dimethylamino)methanol (DMAM) was then triggered by the addition of H_2 to

Table 1: Summary of thermodynamic and kinetic data associated with all catalytic cycles forming either MeOH or TMA. Values are reported in the gas phase in units of kcal/mol using LANL2DZ/B3LYP level of theory, relative to the energy of the starting material (**1**, DMC, etc.

Cycle number	Activation energy ($\Delta G^{\ddagger}$)	Lowest energy intermediate
1 (MeOH)	86.7	**1** (-144.0)
1 (TMA)	94.8	**1** (-147.6)
2	59.1	**15** (-170.4)
3 (MeOH)	59.1	**1** (-132.8)
3 (TMA)	59.1	**15** (-174.0)
4 (MeOH)	34.5	**1** (-109.0)
4 (TMA)	34.5	**36** (-128.1)
5	38.7	**1** (-156.8)

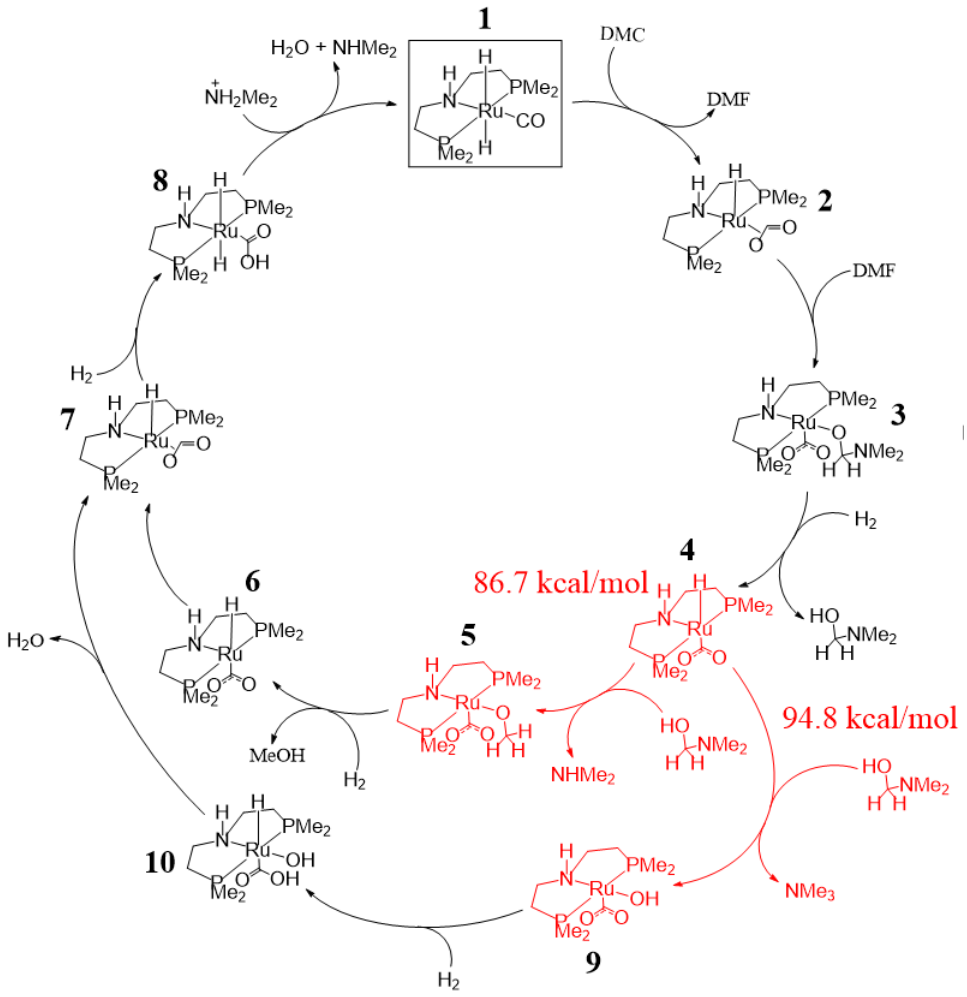

Figure 11: Full reaction mechanisms for pathways forming MeOH (top) and TMA (bottom), as identified in **Cycle 1**. Corresponding rate-limiting steps are shown in red in each case and overall activation energies are also displayed (gas phase; LANL2DZ/B3LYP).

Ru followed by proton transfer to the oxygen atom, resulting in **4**. The next step involved another hydride transfer from Ru to O, which forced the dissociation of $NHMe_2$ due to the full saturation of the carbon atom in DMAM, leaving a methoxy ligand bound to the metal center in **5**. The subsequent release of MeOH proved rather facile, as it merely required the addition of a second H_2 molecule followed by oxygen protonation. Even though the product of interest was successfully formed, the pathway still needed to regererate the catalyst. Because the carbonyl ligand in **1** is positioned equatorially, the carbon dioxide ligand was forced to move from an axial position in **6** to an equatorial one in in **7**. We then added a third H_2 molecule to insert the missing hydride and protonate the carbon dioxide ligand in **8**. Finally, $NH_2Me_2^+$ was combined with the complex to protonate the carbon dioxide ligand a second time, triggering the release of water and leaving behind **1**.

During the process of elucidating **Cycle 1**, we also noticed the ability of an alternative product to be formed. Rather than losing a C-N bond, DMAM could receive a hydride from Ru and instead break the C-O bond, knocking off the hydroxide ion, which then binds to the metal center, resulting in the release of trimethylamine (TMA), one of the side products identified experimentally. Following TMA formation, addition of H_2 protonates the hydroxy ligand, forcing the dissociation of water. The catalyst is subsequently regenerated in the same fashion as in the MeOH pathway.

It is clear that **Cycle 1**, whether it produces MeOH or TMA, is unlikely to be energetically feasible, as the rate-determining step involving re-insertion of DMAM followed by hydride transfer from Ru to the sp^3C appeared to have gas-phase energies far beyond the threshold calculated above. While the minimum expected activation energy as determined by **Equation 2** is 39 kcal/mol, the energies associated with MeOH and TMA production, respectively, were as high as $\Delta G^{\ddagger}$=86 and 94 kcal/mol, respectively. It is likely that the DMAM substrate is too bulky to circumvent the crowded environment around the metal center, which has both a carbon dioxide and a hydride attached to it, and that this complication results in a relatively high barrier for this elementary step due to steric hindrance.

3.3. Catalytic Cycle 2

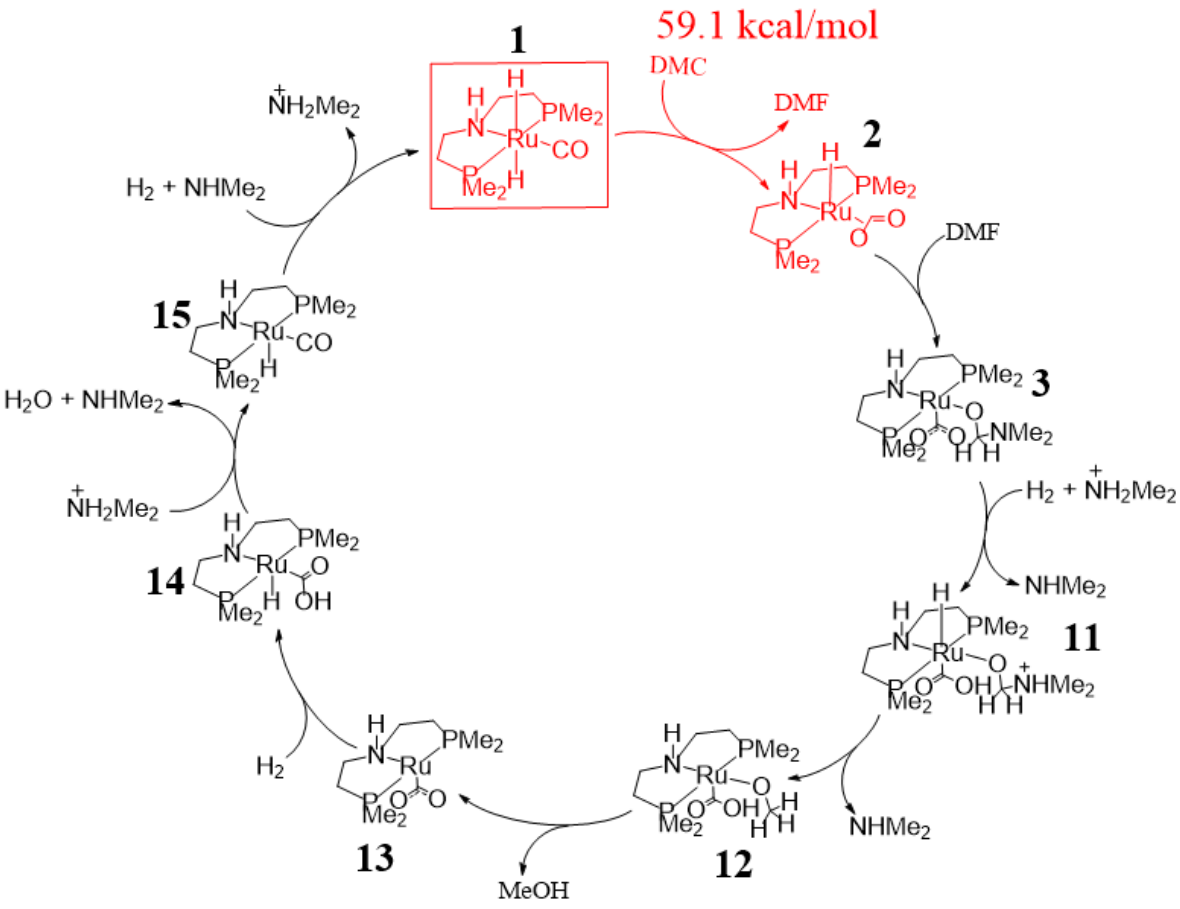

Figure 12: Full reaction mechanism for **Cycle 2**, which was shown to yield MeOH. The rate-limiting step is shown in red in each case and the overall activation energy is also displayed (gas phase; LANL2DZ/B3LYP).

After further exploration, we were able to generate a very similar catalytic cycle for the formation of MeOH, except that DMAM never leaves the complex, but rather transforms into a methoxy ligand while still bound to the metal (**Cycle 2**, **Figure 12**). The key in this mechanism is that the carbon dioxide ligand is protonated early on in the reaction, resulting in stabilizing hydrogen bonding interactions between this ligand and the neighboring oxygen atom of DMAM, as seen in **11** and **12**. Addition of H_2 to **13** resulted in Ru-H bond

formation alongside an equatorial protonated carbon dioxide ligand in **14**. Proton transfer from $NH_2Me_2^+$ to the complex then triggered the release of water from **15**. The resulting intermediate resembles **1** with the exception of a missing hydride. Addition of yet another H_2 molecule to fill this void coupled with proton transfer to $NHMe_2$ resulted in the formation of $NH_2Me_2^+$ and **1**, the initial catalyst. For this cycle, the rate-determining step was identified to be the very first step, namely the conversion of DMC to DMF, with an activation barrier of $\Delta G^{\ddagger}$=59 kcal/mol, which is significantly lower than those of **Cycle 1**.

3.4. Catalytic Cycle 3: MeOH and TMA Pathways

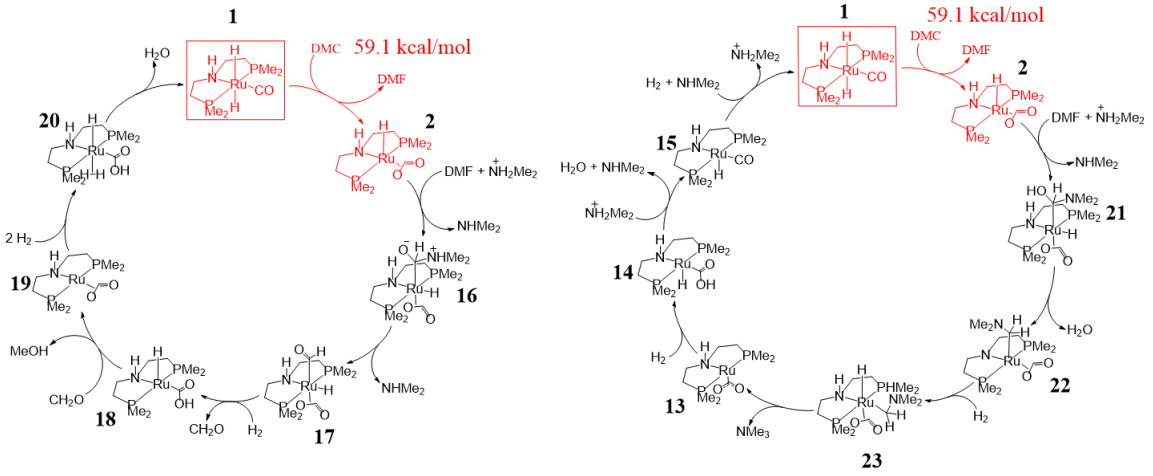

Figure 13: Full reaction mechanisms for pathways forming MeOH (left) and TMA (right), as identified in **Cycle 3**. The rate-limiting step is shown in red in each case and overall activation energies are also displayed (gas phase; LANL2DZ/B3LYP).

A third mechanism for producing MeOH was also elucidated, involving this time the binding of DMF to the metal through carbon rather than the oxygen in **16** (**Cycle 3**, **Figure 13**). The rate-limiting step in this cycle was found to be the initial DMF formation step, as in **Cycle 2**. It was found that the DMF ligand could become once again sp^2-hybridized by losing $NHMe_2$, resulting in a formyl ligand in **17**. The transfer of a hydride to this carbon center then triggers the release of formaldehyde. **18** simultaneously donates

a hydride and a proton to formaldehyde, leaving behind **19** and MeOH. The addition of two H_2 molecules then regenerates the two missing hydrides in the complex and helps converts the carbon dioxide ligand back to a carbonyl ligand. It was discovered for this particular cycle that TMA formation was also possible, with slight alterations to the mechanism. In this case, the oxygen of DMF gets protonated rather than the nitrogen. A proton transfer between the N-H group in **21** and the adjacent hydroxide, as well as a hydride transfer from the ruthenium center to the sp^3C, results in the loss of a water molecule from **22**. Addition of H_2 helps regenerate the N-H group in **23** and a subsequent hydride transfer releases TMA from **13**. From this observation it is possible that the presence of the N-H group positively influences TMA production over MeOH production, on which it has a minor impact. Addition of H_2 to replace the missing hydride and regain the N-H group then causes TMA to leave the complex. Catalyst regeneration proceeds this time exactly as it did with **Cycle 2**.

3.5. Catalytic Cycle 4: MeOH and TMA Pathways

Even though the aforementioned mechanisms have activation barriers which are much lower than those of **Cycle 1**, there exist cycles that are even more kinetically favorable. We hypothesized that the initial formation of DMF need not occur in one single step. It is likely that direct σ-bond metathesis is not a favorable approach to breaking one of the C-O bonds in DMC. We noticed a different initial step in the new mechanism, namely the binding of DMC to the metal center of **1** through one of its oxygen atoms (**Cycle 4**, **Figure 14**). In order to preserve the octahedral environment around Ru, one of the hydrides was observed to migrate toward the carbonyl ligand, making room for the substrate. Next, an oxidative addition-like step occurs, where the metal center ends up attached to both the carbon atom initially present and a hydroxy ligand in **25**. Because a seven-coordinate Ru complex is unfavorable, the loss of the Ru-N bond was seen to take place during this step. A hydride

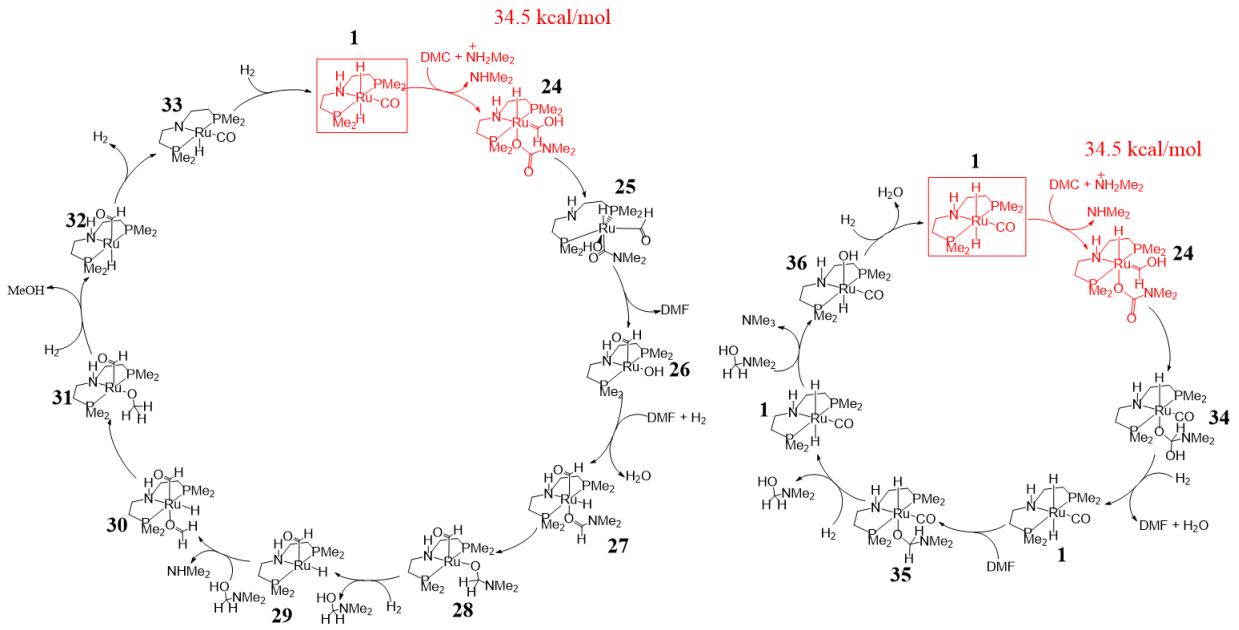

Figure 14: Full reaction mechanisms for pathways forming MeOH (left) and TMA (right), as identified in **Cycle 4**. The rate-limiting step is shown in red in each case and overall activation energies are also displayed (gas phase; LANL2DZ/B3LYP).

shift from Ru to the sp^2C subsequently forces the release of DMF from **26**. Addition of H_2 adds a hydride to the ruthenium center and protonates the hydroxy ligand, releasing water, before DMF binds to Ru, triggering a hydride shift from the metal to the sp^2C. This step of the mechanism also involved re-binding of Ru to the N-H group of the ligand. This reaction pathway further provides evidence for the importance of the N-H group in providing stability of the complex while interacting with DMF. Addition of a second H_2 molecule creates a new Ru-H bond and causes the dissociation of DMAM, which breaks down into $NHMe_2$ and formaldehyde. The latter intermediate then binds back to Ru in **30** through its oxygen atom and receives the hydride from the ruthenium center. A third H_2 molecule then adds yet another Ru-H bond and releases MeOH from **32**. The challenge was then to force the formyl ligand back to an equatorial position, as the oxygen atom appeared to interact with the neighboring N-H group via hydrogen bonding, thus stabilizing the axial arrangement. Interestingly enough, the simplest way to accomplish this was to rotate the formyl ligand and release H_2, forcing the resulting carbonyl to an equatorial arrangement, as seen in **33**.

Re-addition of H_2 finally filled the remaining voids needed to reconstruct **1**.

An alternate pathway to form TMA was found to occur as described in **Cycle 4**. This cycle initially involves the binding of DMC to **1**, as in the MeOH pathway described above. This time, however, a hydride shift occurs from the formyl ligand in **24** to the sp^2C, followed by the addition of H_2, which adds a hydride back to Ru and triggers the dissociation of (dimethylamino)methanediol. Interestingly, this new species spontaneously decomposes to water and DMF. DMF then receives a hydride from Ru and subsequently binds to the complex through its oxygen atom. As in the MeOH case, addition of H_2 results in the release of DMAM, which is then involved in σ-bond metathesis with the complex. This facile exchange of hydroxide in DMAM with a hydride bound to Ru yields TMA and **36**. At last, a third H_2 molecule protonates the resulting hydroxy ligand, releasing water, and adds the missing Ru-H bond. Hence it is clear that we have found a means of producing an undesired chemical species with a low enough energy of activation, showing the inability of the complex to selectively form MeOH. In both MeOH and TMA pathways, the rate-determining step was found to be the initial formation of the Ru-DMC adduct and the kinetic barrier was in both cases found to be a much more favorable $\Delta G^{\ddagger}$=34 kcal/mol.

3.6. Catalytic Cycle 5

From all above pathways, it is clear that DMF represents a viable intermediate toward MeOH formation. In a separate cycle, DMF formation occurred in a similar fashion as in **Cycle 4**, except cleavage of the Ru-N bond in **1** occurs before binding of the DMC substrate (**Cycle 5**, **Figure 15**). As in the previous cycle, this step was rate-limiting, with a transition state energy relative to the starting point comparable to that of the other pathway ($\Delta G^{\ddagger}$=38 kcal/mol). Because of the loss of the Ru-N bond, both hydrides were this time able to remain intact, as seen in **37**. The next step then resembles an oxidative addition, as one of the C-O bonds of DMC breaks, followed by binding of Ru to the electrophilic carbon atom and migration of the lone oxide to the carbonyl ligand in **38**. This step is reminiscent of the rate-

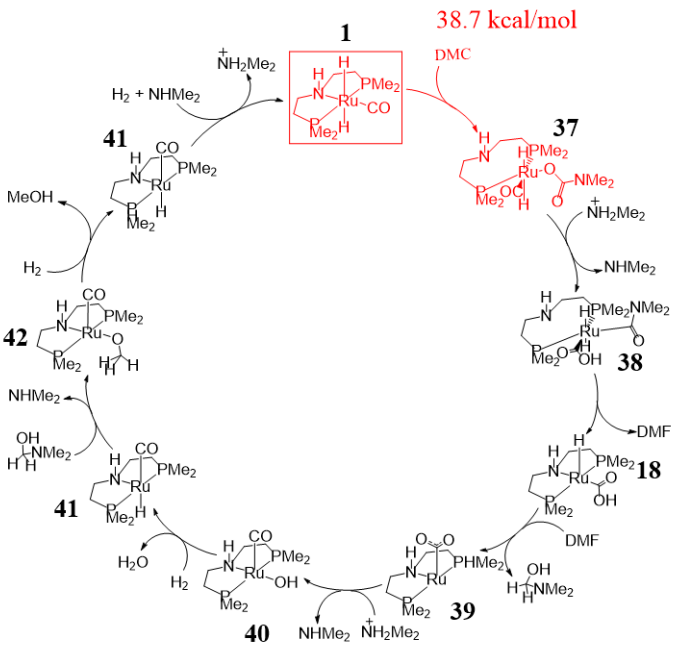

Figure 15: Full reaction mechanism for **Cycle 5**, which was shown to yield MeOH. The rate-limiting step is shown in red in each case and the overall activation energy is also displayed (gas phase; LANL2DZ/B3LYP).

limiting step of **Cycle 2** and **Cycle 3**, except that the loss of oxide from DMC is assisted by formation of the complex-substrate adduct. One cannot therefore deny the catalytic activity of the metal complex, as it successfully lowers the energy of activation for this step in particular. A hydride shift from the metal to the sp^2C triggers the release of DMF from **18**. Upon re-entry, DMF immediately transforms to DMAM with the help of a hydride transfer, leaving behind **39**. The proton adjacent to the oxygen originates from a $NH_2Me_2^+$ ion introduced in an earlier step. Addition of this ion once again causes the protonation of the carbon dioxide ligand, which undergoes oxidative addition, leaving behind a carbonyl ligand as well as a hydroxy ligand. Adding H_2 then inserts a hydride to **40** and results in the dissociation of water from **41**. The new hydride then migrates to the DMAM intermediate, which binds to Ru through its oxygen atom and from which $NHMe_2$ subsequently dissociates. The resulting methoxy ligand in **42** is protonated via addition of H_2 and MeOH is allowed to leave the system. Catalyst regeneration finally proceeds in the same manner as in **Cycle 2**. What is interesting about this cycle is that relative to the MeOH pathway of **Cycle 4**,

this one involves a much lower dip in energy between the start and end of one full cycle (ΔG=-156 kcal/mol as opposed to -109 kcal/mol), even though the kinetic barrier is slightly higher in energy, yet still within experimental reason.

3.7. Cycle Comparisons and Differences in Energetics

The pathways shown in **Figure 16a** involve the formation of MeOH with an overall energy barrier exceeding the approximated threshold. Both cycles had the same rate-limiting step ($\Delta G^{\ddagger}$=59 kcal/mol), corresponding to the one-step conversion of DMC to DMF. Still, both cycles avoid the much higher energy barrier seen in **Cycle 1**, which occurred later in the pathway. The reason for this is unlike **Cycle 1**, **Cycle 2** and **Cycle 3** both drop steeply in energy early in the pathway. In the former case, the path is observed to significantly go down in energy between **3** and **11** (for this elementary step, $\Delta G^{\ddagger}$=21 kcal/mol and ΔG=-134 kcal/mol), likely due to the appearance of a hydrogen bonding interaction between two neighboring ligands. In the latter case, however, formation of the Ru-C bond following DMF formation is highly exothermic, resulting in the sharp energy decrease from **2** to **16** (for this elementary step, $\Delta G^{\ddagger}$=18 kcal/mol and ΔG=-132 kcal/mol). In both cases, the energy already reaches more than 80 kcal/mol below the starting point and the energy remains low enough to circumvent any barriers associated with subsequent elementary steps. A striking difference between the two cycles is that the hydride transfer resulting in formaldehyde release in **Cycle 3** has a barrier of 87 kcal/mol, which is significantly higher than that of the hydride transfer forming a methoxy ligand in **Cycle 2**, which is 28 kcal/mol. This discrepancy could stem from the fact that formation of **18** results in the loss of a Ru-C bond whereas **12** formation keeps the Ru-O bond intact, meaning there is a significant difference in enthalpy change between the two cycles in this step. Finally, **Cycle 2** is more thermodynamically favorable than **Cycle 3** (after catalyst regeneration, -160 versus -132 kcal/mol), which is primarily due to the significant decrease in energy during the step between **13** and **14** ($\Delta G^{\ddagger}$=59 kcal/mol, ΔG=-41 kcal/mol) relative to that between **19**

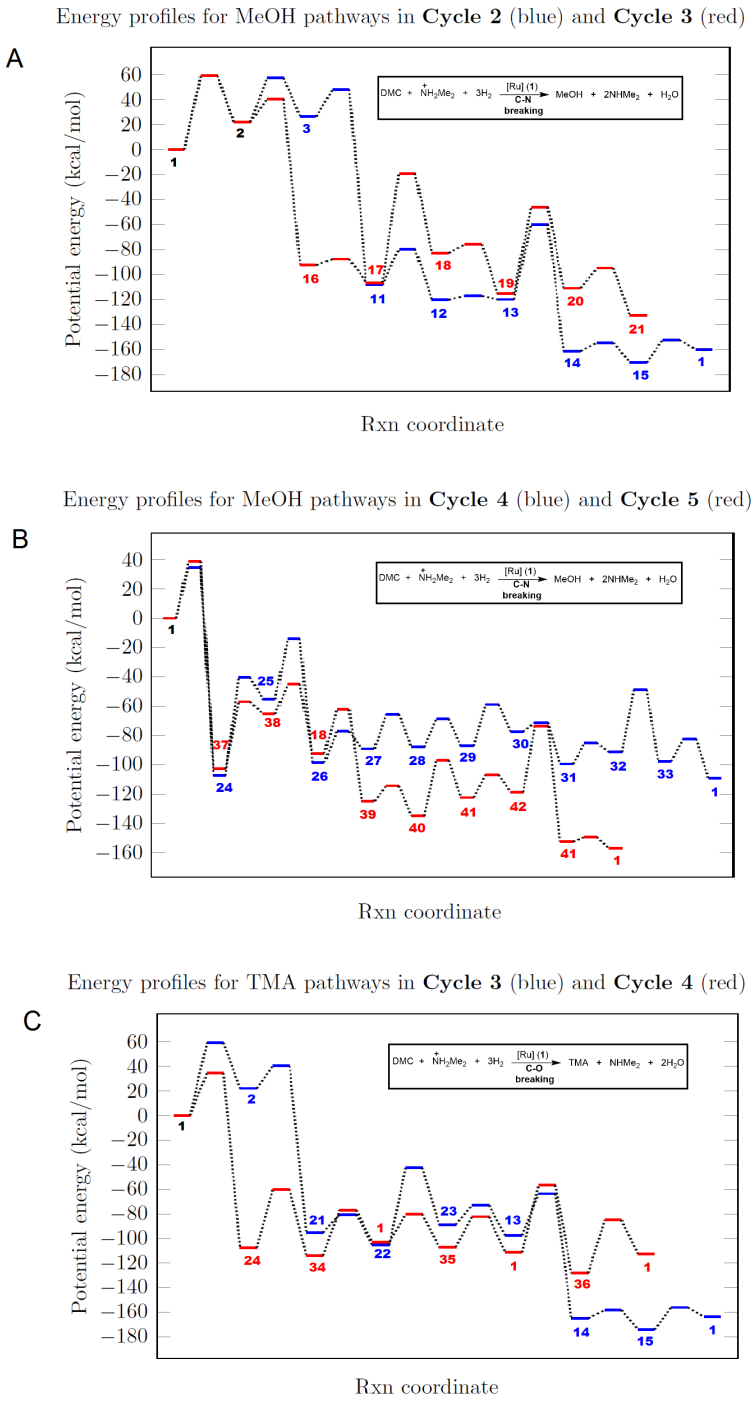

Figure 16: Energy profiles for each reaction mechanism elucidated via DFT for conversion of DMC to MeOH (a, high barrier; b, low barrier) or TMA (c). Each node is labeled with a specific complex, whose number can be found in **Figures 11-15**. **Cycle 1** mechanisms were omitted due to high kinetic barriers (**Table 1**). All energies are reported in the gas phase using LANL2DZ/B3LYP level of theory.

and **20** ($\Delta G^{\ddagger}$=69 kcal/mol, ΔG=+4 kcal/mol). Both **14** and **20** reveal the possibility of hydrogen bonding, although the latter structure is much more crowded around the metal, likely hindering the stabilizing interaction between the carbon dioxide and the dihydrogen ligand due to steric hindrance.

As described in earlier subsections, the pathways laid out in **Figure 16b** have significantly lower activation energies than **Cycle 2** or **Cycle 3** ($\Delta G^{\ddagger}$=34 and 38 kcal/mol for **Cycle 4** and **Cycle 5**, respectively), which is likely the result of multi-step DMF formation. In both cases, a thermodynamic sink occurs already in the first step, namely the formation of a Ru-O bond, perhaps a highly exothermic process. The main difference in the first few steps between the two cycles is that in **Cycle 4** the loss of a Ru-H bond makes way for the the DMC substrate, while in **Cycle 5** it is cleavage of the Ru-N bond that allows DMC to bind to the metal. Perhaps the loss of Ru-N is what accounts for the slight discrepancy in activation energies between the two cycles. As noted in earlier subsections, even though the kinetic barrier of **Cycle 5** is slightly higher than that of **Cycle 4**, **Cycle 5** is significantly more exergonic (after catalyst regeneration, -142 versus -108 kcal/mol). This difference in free energy change stems primarily from two particular steps, namely the conversion of **18** to **39** ($\Delta G^{\ddagger}$=30 kcal/mol, ΔG=-32 kcal/mol) and from **42** to **41** ($\Delta G^{\ddagger}$=45 kcal/mol, ΔG=-33 kcal/mol). In the former step, the carbon dioxide moves to an axial position and is therefore stabilized through van der Waals interactions with the neighboring N-H group. The latter step, on the other hand, involves the release of MeOH, which relieves a considerable amount of crowdedness around the metal center. Given that this gives the axial carbonyl ligand more freedom as it can now easily take various positions, the entropy change associated with this step should be rather large. In **Cycle 4**, the formyl ligand remains near the N-H group since the early conversion of **25** to **26** ($\Delta G^{\ddagger}$=41 kcal/mol, ΔG=-43 kcal/mol) and no subsequent step is able to contribute further van der Waals interactions. Furthermore, in the conversion from **31** to **32** ($\Delta G^{\ddagger}$=14 kcal/mol, ΔG=+8 kcal/mol), the formyl ligand is constrained by attractive interactions with the neighboring N-H group, and so it lacks the same level of

freedom that the carbonyl ligand possesses in **41**.

Our analysis would not be complete without the pathways for TMA formation, as shown in **Figure 16c**. The main difference between the two cycles is that **Cycle 3** involves one-step DMF formation and therefore has a high kinetic barrier, while **Cycle 4** forms DMF on the third elementary step, after binding of DMC to the ruthenium complex. As in MeOH pathways discussed above, thermodynamic sinks early on in the mechanism ensure that the energy is kept low enough to overcome any subsequent barrier. Highly exergonic steps occur both between **2** and **21** in **Cycle 3** (Ru-C bond formation), with a free energy of -117 kcal/mol, and between **1** and **24** in **Cycle 4** (Ru-O bond formation), with a free energy of -107 kcal/mol. Both elementary steps are likely highly exothermic. The difference in reaction free energy (after catalyst regeration -163 and -112 kcal/mol for **Cycle 3** and **Cycle 4**, respectively) stems most likely from the highly exergonic conversion of **13** to **14** ($\Delta G^{\ddagger}$=33 kcal/mol, ΔG=-67 kcal/mol), which can be explained by the appearance of hydrogen bonding interactions between the carbon dioxide ligand and the neighboring hydride. This stabilizing feature is however not present in any intermediate in **Cycle 4**.

From these catalytic cycles it is not easy to determine whether the ruthenium catalyst coupled with $NHMe_2$ favors the production of MeOH (C-N bond cleavage) over TMA (C-O bond cleavage). Indeed, pairs of analogous pathways forming both products have comparable activation energies, as the rate-determining step occurs early on in the mechanism. The only exception to this is **Cycle 1**, in which the barrier for TMA formation was higher than that of MeOH, an indication that C-O bonds may generally be more difficult to break than C-N bonds. However, in all cycles, formation of TMA led to a lower overall Gibbs free energy change relative to MeOH formation. This could be an indication that over very long periods of time, the reaction may be selective toward TMA formation. It is therefore crucial that the catalyst be modified to increase the energy barriers associated with TMA production to a much higher value than that for MeOH production. The same can be said of DMF formation, as the rate determining step in all cycles except **Cycle 1** occurs either during or before DMF

release. A striking observation is that in some cases, as in the TMA pathway of **Cycle 4**, the catalyst is fully regenerated after DMF formation but prior to TMA formation, and hence the reaction forming DMF has the exact same energy barrier as the reactions forming either of the two products. While there is no evidence for selective formation of DMF over other products, including MeOH, efforts must be made to design a catalyst that can either form DMF, which can eventually transform to MeOH in a rather barrierless transition, or avoid the DMF pathway altogether. Further mechanistic investigations may need to be performed to explore potential MeOH-yielding pathways that forego the release of DMF.

Because the energies listed throughout this report are in the gas phase, one cannot rule out the possibility that inclusion of a solvent model could lower some of the activation barriers discovered. While it is unlikely that **Cycle 1** is energetically feasible, there is still hope for **Cycle 2** as well as **Cycle 3**. Still, there is no doubt that the last two cycles are likely mechanisms for DMC hydrogenation, given that even the gas-phase barrier in both cases lies within the approximated energetic threshold. While formation of MeOH in **Cycle 4** is slightly more kinetically favorable than that in **Cycle 5**, **Cycle 5** has a significantly lower change in Gibbs free energy. Hence, if left for long period of time, **Cycle 5** is more likely to be favored. However, further detailed mechanistic studies of the system will be necessary to test these hypotheses.

4. CONCLUSION

To summarize, this study has demonstrated that the selective tandem Ru- and amine-catalyzed formation of methanol from carbon dioxide is a difficult task given the equivalent favorability of by-products such as trimethylamine and dimethylformamide. Pathways whose barriers are too high to be considered favorable as well as ones with low enough barriers were successfully elucidated via density functional theory using ZStruct/SEGSM for both MeOH and TMA formation. Both products were yielded in separate full catalytic cycles with very comparable energetics, having similar activation barriers and very negative reaction free energy changes. Moreover, in all reaction pathways aside from ones with unreasonably high kinetic barriers, DMF is not released as an intermediate until after the highest energy point is reached. In some cases, the intitial metal complex is even regenerated in between formation of DMF and formation of a different product. Based on the gas-phase energies it is therefore not obvious whether the pathways favor only one hydride shift (DMF) or repeated reduction steps (MeOH or TMA). Of course, the inclusion of a solvent model has the potential to yield vastly different results, which is why solvent calculations prove crucial for a thorough understanding of the system. Further experimental and theoretical investigations will also be needed to explore further means of producing MeOH in low energy pathways while ensuring that by-product formation is kinetically unfeasible. This could either be accomplished with the same complex, with or without replacement of methyl groups with phenyl groups (Ru-MACHO-BH_4) or with a new catalyst whose ligands have been fine-tuned to selectively favor C-N bond cleavage over C-O bond cleavage. Numerous factors such as sterics and van Der Waals interactions must be taken into consideration when designing a new homogeneous catalyst for a complicated reaction medium such as this one. Future work could also revolve around extending our results to additional amine bases with different R groups to illuminate potential trends in reactivity. Properties such as the electron withdrawing or electron donating nature and bulkiness of R groups remain to be elucidated. Such studies may shed some further light on the ease with which certain specific types of bonds are broken over others.

5. ACKNOWLEDGEMENTS

I owe my sincerest gratitude to both my principal investigator, Paul Zimmerman, and my graduate student mentor, Amanda Dewyer, for countlessly aiding me throughout my research project and for assisting me in the successful completion of this thesis. They have both proved instrumental in helping me gain a thorough understanding of the various methodologies employed in the research group, including the ones used in my work. Special thanks to Paul Zimmerman, Bart Bartlett, Mark Banaszak Holl, and Stephen Maldonado, for all the guidance they have provided me throughout my undergraduate years and for advocating in my behalf for opportunities in graduate study. I would also like to thank Amanda Dewyer for being both a knowledgeable mentor and a good friend and Alan Chien for very insightful discussions regarding post-undergraduate opportunities and graduate student life. Finally, my academic growth and success would not be possible without the constant love and support of my parents, Gabriela and Jon, from early childhood to the end of a marvelous four years here at the University of Michigan.

6. REFERENCES

(1) Kamijo, T.; Sorimachi, Y.; Shimada, D.; Miyamoto, O.; Endo, T.; Nagayasu, H. *A. Energy Procedia* **2013**, *37*, 813.

(2) Figueroa, J. D.; Fout, T.; Plasynski, S.; McIlvried, H.; Srivastava, R. D. *Int. J. Greenh. Gas Control* **2008**, *2*, 9.

(3) Yang, H.; Xu, Z.; Fan, M.; Gupta, R.; Slimane, R. B.; Bland, A. E.; Wright, I. *J. Environ. Sci.* **2008**, *20*, 14.

(4) Macdowell, N.; Florin, N.; Buchard, A.; Hallett, J.; Galindo, A.; Jackson, G.; Adjiman, C. S.; Williams, C. K.; Shah, N.; Fennell, P. *Energy Environ. Sci.* **2010**, *3*, 1645.

(5) Benson, E.; Kubiak, C. P.; Sathrum, A. J.; Smieja, J. M. *Chem. Soc. Rev.* **2009**, *38*, 89–99.

(6) Morris, A. J.; Meyer, G. J.; Fujita, E. *Acc. Chem. Res.* **2009**, *42*, 1983–1994.

(7) Rakowski DuBois, M.; DuBois, D. L. *Acc. Chem. Res.* **2009**, *42*, 1974–1982.

(8) Takeda, H.; Ishitani, O. *Coord. Chem. Rev.* **2010**, *254*, 346–354.

(9) Tamaki, Y.; Morimoto, T.; Koike, K.; Ishitani, O. *Proc. Natl. Acad. Sci. U. S. A.* **2012**, *109*, 15673–15678.

(10) Tamaki, Y.; Koike, K.; Morimoto, T.; Ishitani, O. *J. Catal.* **2013**, *304*, 22–28.

(11) Sato, S.; Arai, T.; Morikawa, T.; Uemura, K.; Suzuki, T. M.; Tanaka, H.; Kajino, T. *J. Am. Chem. Soc.* **2011**, *133*, 15240–15243.

(12) Arai, T.; Sato, S.; Uemura, K.; Morikawa, T.; Kajino, T.; Motohiro, T. *Chem. Commun.* **2010**, *46*, 6944–6946.

(13) Yamanaka, K.-i.; Sato, S.; Iwaki, M.; Kajino, T.; Morikawa, T. *J. Phys. Chem. C* **2011**, *115*, 18348–18353.

(14) Sekizawa, K.; Maeda, K.; Domen, K.; Koike, K.; Ishitani, O. *J. Am. Chem. Soc.* **2013**, *135*, 4596–4599.

(15) Nielsen, M.; Alberico, E.; Baumann, W.; Drexler, H.-J.; Junge, H.; Gladiali, S.; Beller, M. *Nature* **2006**, *495*, 85–89.

(16) Jia, G.; Tan, Y.; Han, Y. *Ind. Eng. Chem. Res.* **2006**, *45*, 1152–1159.

(17) Leitner, W. *Angew. Chem.* **1995**, *34*, 2207–2221.

(18) Waller, D.; Stirling, D.; Stone, F. S.; Spencer, M. S. *Faraday, Discuss. Chem. Soc.* **1989**, *87*, 107.

(19) Spencer, M. S. *Top. Catal.* **1999**, *8*, 259.

(20) Grabow, L. C.; Mavrikakis, M. *ACS Catal.* **2011**, *1*, 365.

(21) Tedsree, K.; Li, T.; Jones, S.; Chan, C. W. A.; Yu, K. M. K.; Bagot, P. A. J.; Marquis, E. A.; Smith, G. D. W.; Tsang, S. C. E. *Nat. Nanotechnol.* **2011**, *6*, 302–307.

(22) Zhu, Q.-L.; Tsumori, N.; Xu, Q. *Chem. Sci.* **2014**, *5*, 195–199.

(23) Wang, W.; Wang, S.; Ma, X.; Gong, J. *Chem. Soc. Rev.* **2011**, *40*, 3703–3727.

(24) Gassner, F.; Leitner, W. *J. Chem. Soc., Chem. Commun.* **1993**, 1465–1466.

(25) Elek, J.; Nadasdi, L.; Papp, G.; Laurenczy, G.; JooÌĄ, F. *Appl. Catal., A* **2003**, *255*, 59–67.

(26) Laurenczy, G.; Joó, F.; Nadasdi, L. *Inorg. Chem.* **2000**, *39*, 5083–5088.

(27) Horvath, H.; Laurenczy, G.; Katho, A. *J. Organomet. Chem.* **2004**, *689*, 1036–1045.

(28) Erlandsson, M.; Landaeta, V. R.; Gonsalvi, L.; Peruzzini, M.; Phillips, A. D.; Dyson, P. J.; Laurenczy, G. *Eur. J. Inorg. Chem.* **2008**, *2008*, 620–627.

(29) Laurenczy, G.; Jedner, S.; Alessio, E.; Dyson, P. J. *Inorg. Chem. Commun.* **2007**, *10*, 558–562.

(30) Federsel, C.; Ziebart, C.; Jackstell, R.; Baumann, W.; Beller, M. *Chem. - Eur. J.* **2012**, *18*, 72–75.

(31) Ziebart, C.; Federsel, C.; Anbarasan, P.; Jackstell, R.; Baumann, W.; Spannenberg, A.; Beller, M. *J. Am. Chem. Soc.* **2012**, *134*, 20701–20704.

(32) Schmeier, T. J.; Dobereiner, G. E.; Crabtree, R. H.; Hazari, N. *J. Am. Chem. Soc.* **2011**, *133*, 9274–9277.

(33) Han, Z.; Rong, L.; Wu, J.; Zhang, L.; Wang, Z.; Ding, K. *Angew. Chem., Int. Ed.* **2012**, *51*, 13041–13045.

(34) Huff, C. A.; Sanford, M. S. *J. Am. Chem. Soc.* **2011**, *313*, 18122–18125.

(35) Kumar, N.; Camaioni, D. M.; Dupuis, M.; Raugei, S.; Appel, A. *Dalton Trans.* **2014**, *43*, 11803–11806.

(36) Filonenko, G. A.; Hensen, E. J. M.; Pidko, E. A. *Catal. Sci. Technol.* **2014**, *4*, 3474–3485.

(37) Filonenko, G. A.; Conley, M. P.; Coperet, C.; Lutz, M.; Hensen, E. J. M.; Pidko, E. A. *ACS Catal.* **2013**, *3*, 2522–2526.

(38) Suna, Y.; Ertem, M. Z.; Wang, W.-H.; Kambayashi, H.; Manaka, Y.; Muckerman, J. T.; Fujita, E.; Himeda, Y. *Organometallics* **2014**, *33*, 6519–6530.

(39) Hou, C.; Jiang, J.; Zhang, S.; Wang, G.; Zhang, Z.; Ke, Z.; Zhao, C. *ACS Catal.* **2014**, *4*, 2990–2997.

(40) Yang, L.; Wang, H.; Zhang, N.; Hong, S. *Dalton Trans.* **2013**, *42*, 11186–11193.

(41) Yang, X. *ACS Catal.* **2012**, *2*, 964–970.

(42) Balaraman, E.; Gunanathan, C.; Zhang, J.; Shimon, L. J. W.; Milstein, D. *Nat. Chem.* **2011**, *3*, 609–614.

(43) Rezayee, N. M.; Huff, C. A.; Sanford, M. S. *J. Am. Chem. Soc.* **2015**, *137*, 1028–1031.

(44) Cramer, C. J. *Essentials of Computational Chemistry: Theories and Models*, 2nd ed.; Wiley: United Kingdom, 2004.

(45) Sholl, D. S.; Steckel, J. A. *Density Functional Theory: A Practical Introduction*, 1st ed.; Wiley: Hoboken, NJ, 2009.

(46) Head-Gordon, M. et al. *Mol. Phys.* **2015**, *113*, 184–215.

(47) Zimmerman, P. *J. Comput. Chem.* **2015**, *36*, 601–611.

(48) Zimmerman, P. M. *J. Chem. Phys.* **2013**, *138*, 184102.

(49) Zimmerman, P. M. *J. Chem. Theory Comput.* **2013**, *9*, 3043–3050.

(50) Zimmerman, P. *J. Comput. Chem.* **2013**, *34*, 1385–1392.

(51) Dewyer, A. L.; Zimmerman, P. M. *Org. Biomol. Chem.* **2017**, *15*, 501–504.

(52) Zimmerman, P. M. *Mol. Simul.* **2015**, *41*, 43.

(53) Khomutnyk, Y. Y.; Arguelles, A. J.; Winschel, G. A.; Sun, Z.; Zimmerman, P. M.; Nagorny, P. *J. Am. Chem. Soc.* **2016**, *138*, 444.